HHS Public Access

Author manuscript

Bioconjug Chem. Author manuscript; available in PMC 2017 February 06.

Published in final edited form as:

Bioconjug Chem. 2015 August 19; 26(8): 1470–1474. doi:10.1021/acs.bioconjchem.5b00343.

Nanostar clustering improves the sensitivity of plasmonic assays

Yong Park Il[1], **Hyungsoon Im**[1], **Ralph Weissleder**[1,2], and **Hakho Lee**[1]

[1]Center for Systems Biology, Massachusetts General Hospital, Harvard Medical School, Boston, MA 02114

[2]Department of Systems Biology, Harvard Medical School, Boston, MA 02115

Abstract

Star-shaped Au nanoparticles (Au nanostars, AuNS) have been developed to improve the plasmonic sensitivity, but their application has largely been limited to single-particle probes. We herein describe a AuNS clustering assay based on nanoscale self-assembly of multiple AuNS and which further increases detection sensitivity. We show that each cluster contains multiple nanogaps to concentrate electric fields, thereby amplifying the signal via plasmon coupling. Numerical simulation indicated that AuNS clusters assume up to 460-fold higher field density than Au nanosphere clusters of similar mass. The results were validated in model assays of protein biomarker detection. The AuNS clustering assay showed higher sensitivity than Au nanosphere. Minimizing the size of affinity ligand was found important to tightly confine electric fields and improve the sensitivity. The resulting assay is simple and fast, and can be readily applied to point-of-care molecular detection schemes.

Localized surface plasmon resonance (LSPR) is a promising biosensing strategy for molecular detection.[1–4] Based on surface plasmons that are tightly confined on metallic nanoparticles, LSPR is highly sensitive to changes in dielectric environment surrounding the particles. This unique property has been exploited to detect molecular targets upon their binding to nanoparticle surface.[5–8]

The most widely-used LSPR materials are noble metal (Ag, Au) nanospheres; their synthetic methods are well established and these particles show plasmon resonance in visible wavelengths.[9] Recently, star-shaped nanoparticles (nanostars) have been explored as an alternative substate to improve the LSPR sensitivity. Nanostars have multiple branches with sharp tips that generate more localized electromagnetic fields than do spherical nanoparticles, and thereby produce larger spectral changes upon molecular binding.[10–18] Indeed, Au nanostars have shown >5-fold higher sensitivity than Au nanospheres in LSPR sensing.[19,20] Most previous studies, however, used nanostars as single-particle LSPR probes.[10,13] Namely, the analytical signal was generated when individual nanostars were

*Corresponding authors: R. Weissleder, MD, PhD, H. Lee, PhD, Center for Systems Biology, Massachusetts General Hospital, 185 Cambridge St, CPZN 5206, Boston, MA, 02114, 617-726-8226, rweissleder@mgh.harvard.edu, hlee@mgh.harvard.edu.

Supporting Information

Figure S1–S9 and Table S1. This material is available free of charge via the Internet at http://pubs.acs.org.

labeled with target molecules. We hypothesized that the plasmonic signal could be further amplified by inducing the formation of nanostar clusters. This configuration would create multiple nanogaps between nanostars, wherein electric fields are concentrated and plasmons are coupled.

We herein report on the development and the optimization of such a clustering assay. Using Au nanostars (AuNS) as a substrate, we designed an assay wherein target molecules assemble AuNS into nanoscale-clusters with nanogap junctions. Small AuNS (70 nm in size) with thiolated ligand were found optimal for sensitive and stable plasmonic sensing. Numerical simulation (finite-difference time-domain/FDTD) showed that a cluster of AuNS can concentrate up to 460-fold higher energy density than an Au nanosphere cluster. We then experimentally verified the results using different molecular interactions (i.e., biotin-avidin and antigen-antibody). The AuNS clustering assay produced much larger spectral shifts than AuNS-ligand alone. Notably, the signal improvement inversely depended on the inter-particle distance, which highlighted the importance of minimizing the size of the capturing ligand. The developed assay benefits from fast binding kinetics (<30 min) and a simple signal readout (colorimetry), and could be a potential tool for point-of-care molecular detection.

To synthesize AuNS, we adopted a seed-mediated growth method (see Experimental Section).[21] Spherical Au nanoparticles (AuNP) with a mean diameter of 13 nm were prepared as a seed (Figure 1a, left)[22] and dispersed in an Au precursor ($HAuCl_4$) solution. Star-shaped Au nanoparticles with multiple branches were formed when ascorbic acid and silver nitrate were injected into the seed solution (Figure 1a, right). The reaction was rapid (<1 min for completion) and produced AuNS with size variations of <30% (Figure S1). We further controlled the overall size of AuNS by changing the molar concentration ratio between Au^{3+} and AuNP seeds ($[Au^{3+}]/[AuNP]$). Higher $[Au^{3+}]/[AuNP]$ ratios led to the synthesis of larger AuNS (Figure 1b and S2). When the ratio was $>2\times10^7$, Au precursors spontaneously nucleated, resulting in a mixed phase of AuNP and AuNS (Figure S2). Larger AuNS exhibited a LSPR peak at longer wavelength (Figure 1c and d), because they support more extended longitudinal plasmon resonance along their branches.[23] The peak width also broadened with the particle size (Figure S3), which was likely due to the increasing polydispersity (different branch length and number of branches per particle).

As-synthesized bare AuNS were found spectrally unstable; the sharp tips with high surface energy were susceptible to atomic reorganization, which resulted in the shift of the LSPR peaks to shorter wavelengths (Figure 1e).[24–26] We reasoned that thiol-based ligands could stabilize AuNP by forming a covalent bond with surface Au atoms. Indeed, when AuNS were coated with thiol ligands (e.g., lipoic acid, 11-mercaptoundecanoic acid/MUA, thiolated-polyethylene glycol/PEG), the particles maintained their LSPR peak positions (>12 hrs in phosphate-buffered saline) (Figures 1e and S4).

We next characterized the LSPR properties of individual AuNS. The refractive index sensitivity (RIS) was determined by measuring spectral shifts of particles suspended in solutions of different refractive indices. Water and dimethyl sulfoxide were mixed at varying volume ratios to control the refractive index (see Experimental Section). The measured RIS

of AuNS increased with the overall particle size, ranging from 250 to 500 nm/RIU (refractive index unit, Figure 2a). With similar particle volume, AuNS showed higher RIS than AuNP, validating the advantage of forming sharp branches. For example, the sensitivity of 66 nm AuNS (241 nm/RIU) was 3-fold higher than that of 40 nm spherical AuNP (70 nm/RIU). We also compared the figure of merit (FOM) of particles, that was defined as RIS divided by the full width at half maximum of the LSPR peak (Figure 2b). Particles with high FOM are preferred as they improve the LSPR detection sensitivity.[7,27] Overall, AuNS had higher FOM (~1.8) than spherical AuNP (~0.8). For a given shape, however, the FOM remained similar (coefficient of variation < 12%), because both the RIS and peak-width increased with the particle size. For clustering assays, we thus used small AuNS (~70 nm) for their superior colloidal stability, compared to larger particles.

For molecular sensing with AuNS, we adopted a clustering assay format: AuNS coated with affinity ligands self-assemble into nanoscale clusters in the presence of target molecules (Figure 3a). Such clustering could produce strong plasmonic coupling among AuNS to increase the spectral shift. We first performed a three-dimensional finite-difference time-domain (FDTD) simulation (Figure S5). We calculated the electric-field (*E*-field) of AuNP and AuNS dimers, a simplified version of clusters. The map showed *E*-field concentrated at the junction of two metal particles (Figure 3b). The AuNS dimer showed up to 460-fold higher enhancement than the AuNP dimer (Figure 3c), with *E*-field more efficiently concentrated between tips. The maximum enhancement was observed when two tips of AuNS aligned in a line. Even with misaligned tips, however, the AuNP dimer still showed higher field intensity than the AuNP dimer (Figure S5). The simulation also confirmed that signal amplification could be achieved though particle clustering. Forming a particle-dimer increased the field intensity by 1.7 fold for AuNS (4 fold for AuNP; Figure 3c). Such increases resulted in larger spectral shift ($\Delta\lambda$). The $\Delta\lambda$ for the AuNS dimer, as estimated from the field information, was 2.3-fold larger than AuNS single particle (Figure 3d).

We applied the AuNS clustering assay to detect protein targets. As a model system, we used avidin-biotin interaction, and first compared the detection sensitivity between AuNS and AuNP. Biotinylated particles with similar volumes (AuNP, 40 nm in diameter; AuNS, 70 nm in overall size) were prepared and concentration-matched (see Experimental Section for details). Varying concentrations of avidin were added to particle solutions, and resulting spectral shifts ($\Delta\lambda$) were measured. In the presence of avidin, the particles clustered and their spectral peaks red-shifted (Figure 4a). Dynamic light scattering measurements confirmed the avidin-specific clustering; the hydrodynamic diameter increased with avidin concentration (Figure S6). Dark-field microscopy could also detect AuNS clustering.[28] The aggregated particles appeared brighter than individual particles due to the increased scattering cross-section (Figure S7).[28] The microscopy, however, has a limited assay speed and throughput, and requires fine-tuning of particle concentrations to obtain optimal particle numbers in a field-of-view. In all concentrations tested, AuNS showed larger $\Delta\lambda$ than AuNP. For instance, with the addition of 16 nM of avidin, $\Delta\lambda$ = 19 nm for AuNS and $\Delta\lambda$ = 1.5 nm for AuNP. Titration measurements further confirmed the superiority of AuNS over AuNP (Figure 4b), with AuNS displaying a 7-fold lower limit of detection (LOD = 3.4 nM) than AuNP (LOD = 23.4 nM).

We next examined the effect of the inter-particle distance on the clustering assay sensing. Reducing the inter-particle distance (d_{pp}) is crucial in improving the detection sensitivity, since the field enhancement between the tips decreases exponentially with d_{pp} (Figure S8). As a model detection target, we used the kidney injury molecule-1 (KIM1), an urinary protein marker for kidney injury.[29] To control the particle distance, we prepared two types of probes (see Experimental Section): AuNS conjugated with full polyclonal antibodies (Ab-AuNS) and AuNS with half-antibody fragments ($Ab_{1/2}$-AuNS). As a control, we prepared AuNS conjugated with isotype-matched IgG antibodies. The KIM1 titration experiments showed dose-dependent spectral shifts (Figure 4c), with the half-antibody configuration displaying larger spectral shifts than that with the full-antibody probes. When BSA was used as a control analyte, we observed negligible signal changes (Figure S8); this confirmed that the signal changes were due to antibody-antigen specific aggregation. The LOD for $Ab_{1/2}$-AuNS was 2-fold lower than that of Ab-AuNS. We further compared the detection sensitivity as a function of the inter-particle distance (Figure 4d, Table S1). The LOD values were obtained from the titration experiments (Figure 4b and 4c), and d_{pp} was estimated from the lengths of the passivation layer, affinity ligands and target molecules. The avidin-biotin system ($d_{pp} \approx 12$ nm) showed the lowest detection limit (the highest sensitivity), followed by the half-antibody-antigen ($d_{pp} \approx 19$ nm) and the full-antibody-antigen ($d_{pp} \approx 33$ nm) systems. The improved sensitivity (2-fold) with a shorter inter-particle distance is consistent with our numerical simulation data (Figure S9).

In summary, AuNS are promising nanoprobes for plasmonic biosensing. With multiple branched tips at their surface, AuNS can concentrate electromagnetic fields more efficiently compared to spherical particles, and thereby generate larger plasmonic spectral shifts upon molecular binding. In this study, we found three key aspects to improve sensitive biosensing with AuNS, namely 1) a covalent surface coating to maintain particle morphology and its resonance spectra; 2) AuNS clustering to more strongly concentrate electromagnetic energy; and 3) minimizing the inter-particle distance in AuNS clusters. The resulting AuNS assay was simple and fast, as the reaction occurs in bulk solution and the signals can be read out from visual color changes. Compared to the microscopic observation of individual AuNS, the method is also scalable for high throughput detection. We envision that this assay could have potential applications in point-of-care molecular detection.

EXPERIMENTAL PROCEDURES

Materials

Gold(III) chloride trihydrate (≥99.9%), silver nitrate (≥99.0%), ascorbic acid, sodium citrate dihydrate (≥99%), 11-mercaptoundecanoic acid (MUA), 2-mercaptoethylamine (MEA), 2-maleimidoethylamine trifluoroacetate salt (≥95%) were purchased from Sigma-Aldrich. 40 nm spherical gold nanoparticles were purchased from nanoComposix, inc. Methyl-PEG_4-thiol ($MT(PEG)_4$), 1-ethyl-3-(3-dimethylaminopropyl)carbodiimide hydrochloride (EDC), N-hydroxysulfosuccinimide (sulfo-NHS), (+)-biotinyl-3,6,9,-trioxaundecanediamine (amine-PEG_3-biotin), neutavidin protein were purchased from Thermo Scientific. Human KIM1 polyclonal antibody, recombinant human KIM1, normal goat IgG control were purchased from R&D Systems.

Synthesis of gold nanoparticles

The star-shaped gold nanoparticles (Gold nanostars, AuNS) were synthesized using a seed-mediated growth method, as previously reported.[21] First, the seed gold nanoparticles were prepared through citrate reduction of $HAuCl_4$ by the Turkevich method.[22] Sodium citrate (38.8 mM, 50 mL) was added to the boiling $HAuCl_4$ solution (1 mM, 500 mL) under vigorous stirring, and the mixture was refluxed for 15 min. The seed particles (200 μL) were then added to $HAuCl_4$ (0.25 mM, 10 mL) containing HCl (1 M, 10 μL). $AgNO_3$ (2 mM, 100 μL) and ascorbic acid (0.1 M, 50 μL) were sequentially added to the mixture to initiate the particle growth. The reaction was completed in 30 sec, and the as-synthesized AuNS were purified by centrifugation. The precipitated AuNS were redispersed in 8 mL distilled water. The size of AuNS could be controlled by changing the seed amount. Decreasing seed particle concentrations resulted in larger AuNS. The surface of bare AuNS was functionalized with carboxylic acid. NaOH solution (0.5 M, 80 μL) was added to 8 mL of AuNS solution. Then, MUA (20 mM, 0.4 mL in ethanol) and $MT(PEG)_4$ (20 mM, 0.4 mL in ethanol) were added to the AuNS solution under stirring. After overnight incubation, the functionalized AuNS were washed twice and then dispersed in 1 mL distilled water (~1 nM AuNS). The MUA allows to covalently conjugate affinity ligands through EDC coupling and the PEG layer improves surface hydrophilicity and reduces non-specific binding. The size and shape of the AuNS were characterized by using transmission electron microscopy (TEM, JEOL 2100). The number of the AuNS was counted by nanoparticle tracking analysis (NTA). The hydrodynamic size of the AuNS was measured by dynamic light scattering (Zetasizer APS).

Refractive index sensitivity

The refractive index sensitivities (RIS) of the AuNS and AuNP were measured by incubating the nanoparticles in solvents with different refractive indices (n). The solvents were prepared by mixing DMSO (n =1.48) and water (n = 1.33) at different volume ratios. The absorbance spectra of the samples were measured by a microplate reader (Tecan Safire2™). Figure of merit (FOM) was calculated as a ratio of the measured RIS to the full width at half maximum (FWHM) of the corresponding peak.

Preparation of biotinylated gold nanoparticles

EDC (4 mg/mL, 10 μL) and amine-PEG_3-biotin (10 mg/mL, 100 μL) were added to 1 mL of nanoparticle solution, and the mixture was incubated for 2 hrs at room temperature. The particles were washed twice via centrifugation (3000 × g), and dispersed in 1 mL of 10 mM phosphate buffered saline (PBS) solution.

Antibody conjugation

AuNS conjugated with full polyclonal antibodies were prepared by EDC coupling between AuNS and antibodies. EDC (4 mg/mL, 20 μL) and sulfo-NHS (11 mg/mL, 20 μL) were added to 1 mL of nanoparticle solution. The solution was incubated for 15 min at room temperature, and then washed via centrifugation (3000 × g, 4 °C). The activated nanoparticles were dispersed in 1 mL of 10 mM PBS. Antibody (1mg/mL, 20 μL) was mixed with the activated nanoparticles (0.5 mL), and incubated for 2 hrs at room

temperature. The antibody conjugated AuNS were purified by centrifugation (3000 × g), and dispersed in 1 mL of 10 mM PBS. For conjugation with half-antibody fragments, the surface of AuNS was functionalized by maleimide group to make a thioether bond between AuNS and antibody fragments. EDC (4 mg/mL, 20 μL) and sulfo-NHS (11 mg/mL, 20 μL) were added to 1 mL of nanoparticle solution. The reaction solution was incubated for 15 min at room temperature, and then washed twice. 2-maleimidoethylamine (1 mg/mL, 0.25 mL) was added to the AuNS solution, and reacted for 2 hrs at room temperature. After repeated washing, the nanoparticles were dispersed in 1 mL of 10 mM PBS. Thiolated antibody was prepared by cleaving hinge region disulfide bonds in the heavy chains. Antibody (1mg/mL, 30 μL) was mixed with MEA (60 mg/mL, 3 μL), and incubated for 90 min at 37 °C. The thiolated antibody was purified using Zeba™ spin desalting column (7k MWCO, Thermo Scientific), and added to maleimide-AuNS. Following the incubation overnight at 4 °C, the conjugated AuNS were purified by centrifugation, and dispersed in 1 mL of 10 mM PBS.

Titration experiments

Neutravidin solutions (5 μL) at different concentration were mixed with the biotinylated 70 nm AuNS (45 μL, 0.2 nM) and 40 nm AuNP (45 μL, 0.2 nM), and incubated for 30 min at room temperature. 40 nm AuNP was chosen for comparison with AuNS because they have similar particle volume. Three duplicated samples were prepared for triplicate measurements. The absorbance spectra of the samples on a 384 well plate were measured by a microplate reader (Tecan Safire2™). For antibody experiment, KIM1 solutions (5 μL) at different concentration were mixed with AuNS probes (45 μL), and reacted for 30 min at room temperature. Same procedure used in the neutravidin experiment was applied for KIM1 detection. The limit of detection (LOD) was obtained from the titration curve as 3 × standard deviation (s.d.) of background signal.

LSPR analysis

LSPR peak positions were calculated using a custom-built Matlab software by fitting the absorbance peak to a polynomial curve.[30] All measurements were performed in triplicate and the data are displayed as mean ± s.d.

FDTD simulations

3-dimensional finite-difference time-domain (FDTD) simulations were performed using a commercial software package (FDTD solutions, Lumerical). The dimensions of spherical and star nanoparticles were obtained from TEM images (Figure S2). The extinction spectra, field intensity and spectral shift were calculated from a unit cell with a single nanoparticle or dimer. A non-uniform mesh with a minimum grid size of 1 nm was used. The dielectric constants for Au were obtained from reference.[31] The refractive index of the molecules and ligands was set to 1.6.

Supplementary Material

Refer to Web version on PubMed Central for supplementary material.

Acknowledgments

We thank K. Lee for microscopy imaging; H. Shao and H. J. Chung for helpful discussion. This work was supported in part by NIH Grants R01HL113156, R01EB004626, R01EB010011, HHSN268201000044C, U54-CA119349, and T32-CA79443.

References

1. Hutter E, Fendler JH. Exploitation of localized surface plasmon resonance. Adv Mater. 2004; 16:1685–1706.
2. Anker JN, Hall WP, Lyandres O, Shah NC, Zhao J, Van Duyne RP. Biosensing with plasmonic nanosensors. Nat Mater. 2008; 7:442–453. [PubMed: 18497851]
3. Jain PK, Huang X, El-Sayed IH, El-Sayed MA. Noble metals on the nanoscale: optical and photothermal properties and some applications in imaging, sensing, biology, and medicine. Acc Chem Res. 2008; 41:1578–1586. [PubMed: 18447366]
4. Sepulveda B, Angelome PC, Lechuga LM, Liz-Marzan LM. LSPR-based nanobiosensors. Nano Today. 2009; 4:244–251.
5. Haes AJ, Van D RP. A nanoscale optical blosensor: Sensitivity and selectivity of an approach based on the localized surface plasmon resonance spectroscopy of triangular silver nanoparticles. J Am Chem Soc. 2002; 124:10596–10604. [PubMed: 12197762]
6. Sherry LJ, Jin R, Mirkin CA, Schatz GC, Van Duyne RP. Localized surface plasmon resonance spectroscopy of single silver triangular nanoprisms. Nano Lett. 2006; 6:2060–2065. [PubMed: 16968025]
7. Mayer KM, Hafner JH. Localized surface plasmon resonance sensors. Chem Rev. 2011; 111:3828–3857. [PubMed: 21648956]
8. Gao B, Rozin MJ, Tao AR. Plasmonic nanocomposites: polymer-guided strategies for assembling metal nanoparticles. Nanoscale. 2013; 5:5677–5691. [PubMed: 23703218]
9. Lu X, Rycenga M, Skrabalak SE, Wiley B, Xia Y. Chemical synthesis of novel plasmonic nanoparticles. Annu Rev Phys Chem. 2009; 60:167–192. [PubMed: 18976140]
10. Nehl CL, Liao H, Hafner JH. Optical properties of star-shaped gold nanoparticles. Nano Lett. 2006; 6:683–688. [PubMed: 16608264]
11. Hao F, Nehl CL, Hafner JH, Nordlander P. Plasmon resonances of a gold nanostar. Nano Lett. 2007; 7:729–732. [PubMed: 17279802]
12. Senthil K, Pandian Pastoriza-Santos I, Rodriguez-Gonzalez B, Garcia dA, Javier F, Liz-Marzan LM. High-yield synthesis and optical response of gold nanostars. Nanotechnology. 2008; 19:015606. [PubMed: 21730541]
13. Dondapati SK, Sau TK, Hrelescu C, Klar TA, Stefani FD, Feldmann J. Label-free biosensing based on single gold nanostars as plasmonic transducers. ACS Nano. 2010; 4:6318–6322. [PubMed: 20942444]
14. Barbosa S, Agrawal A, Rodriguez-Lorenzo L, Pastoriza-Santos I, Alvarez-Puebla RA, Kornowski A, Weller H, Liz-Marzan LM. Tuning size and sensing properties in colloidal gold nanostars. Langmuir. 2010; 26:14943–14950. [PubMed: 20804155]
15. Guerrero-Martinez A, Barbosa S, Pastoriza-Santos I, Liz-Marzan LM. Nanostars shine bright for you Colloidal synthesis, properties and applications of branched metallic nanoparticles. Curr Opin Colloid Interface Sci. 2011; 16:118–127.
16. Vo-Dinh T, Fales AM, Griffin GD, Khoury CG, Liu Y, Ngo H, Norton SJ, Register JK, Wang HN, Yuan H. Plasmonic nanoprobes: from chemical sensing to medical diagnostics and therapy. Nanoscale. 2013; 5:10127–10140. [PubMed: 24056945]
17. Webb JA, Erwin WR, Zarick HF, Aufrecht J, Manning HW, Lang MJ, Pint CL, Bardhan R. Geometry-Dependent Plasmonic Tunability and Photothermal Characteristics of Multibranched Gold Nanoantennas. J Phys Chem C. 2014; 118:3696–3707.
18. Solis DM, Taboada JM, Obelleiro F, Liz-Marzan LM, Garcia de Abajo FJ. Toward ultimate nanoplasmonics modeling. ACS Nano. 2014; 8:7559–7570. [PubMed: 25077678]

19. Lu W, Singh AK, Khan SA, Senapati D, Yu H, Ray PC. Gold nano-popcorn-based targeted diagnosis, nanotherapy treatment, and in situ monitoring of photothermal therapy response of prostate cancer cells using surface-enhanced Raman spectroscopy. J Am Chem Soc. 2010; 132:18103–18114. [PubMed: 21128627]
20. Yuan H, Liu Y, Fales AM, Li YL, Liu J, Vo-Dinh T. Quantitative surface-enhanced resonant Raman scattering multiplexing of biocompatible gold nanostars for in vitro and ex vivo detection. Anal Chem. 2013; 85:208–212. [PubMed: 23194068]
21. Yuan H, Khoury CG, Hwang H, Wilson CM, Grant GA, Vo-Dinh T. Gold nanostars: surfactant-free synthesis, 3D modelling, and two-photon photoluminescence imaging. Nanotechnology. 2012; 23:075102. [PubMed: 22260928]
22. Turkevich J, Stevenson PC, Hillier J. A Study of the Nucleation and Growth Processes in the Synthesis of Colloidal Gold. Disc Faraday Soc. 1951:55–75.
23. Khoury CG, Vo-Dinh T. Gold Nanostars For Surface-Enhanced Raman Scattering: Synthesis, Characterization and Optimization. J Phys Chem C. 2008; 2008:18849–18859.
24. Im H, Oh SH. Oxidation sharpening, template stripping, and passivation of ultra-sharp metallic pyramids and wedges. Small. 2014; 10:680–684. [PubMed: 24123889]
25. Malinsky MD, Kelly KL, Schatz GC, Van D RP. Chain length dependence and sensing capabilities of the localized surface plasmon resonance of silver nanoparticles chemically modified with alkanethiol self-assembled monolayers. J Am Chem Soc. 2001; 123:1471–1482.
26. Vega MM, Bonifacio A, Lughi V, Marsi S, Carrato S, Sergo V. Long-term stability of surfactant-free gold nanostars. J Nanopart Res. 2014; 16:2729.
27. Joshi GK, McClory PJ, Muhoberac BB, Kumbhar A, Smith KA, Sardar R. Designing Efficient Localized Surface Plasmon Resonance-Based Sensing Platforms: Optimization of Sensor Response by Controlling the Edge Length of Gold Nanoprisms. J Phys Chem C. 2012; 116:20990–21000.
28. Bu T, Zako T, Fujita M, Maeda M. Detection of DNA induced gold nanoparticle aggregation with dark field imaging. Chem Commun. 2013; 49:7531–7533.
29. Waanders F, van Timmeren MM, Stegeman CA, Bakker SJ, van Goor H. Kidney injury molecule-1 in renal disease. J Pathol. 2010; 220:7–16. [PubMed: 19921716]
30. Im H, Sutherland JN, Maynard JA, Oh SH. Nanohole-based surface plasmon resonance instruments with improved spectral resolution quantify a broad range of antibody-ligand binding kinetics. Anal Chem. 2012; 84:1941–1947. [PubMed: 22235895]
31. Palik, ED. Handbook of optical constants of solids. Elsevier; 1998. http://www.sciencedirect.com/science/book/9780125444156

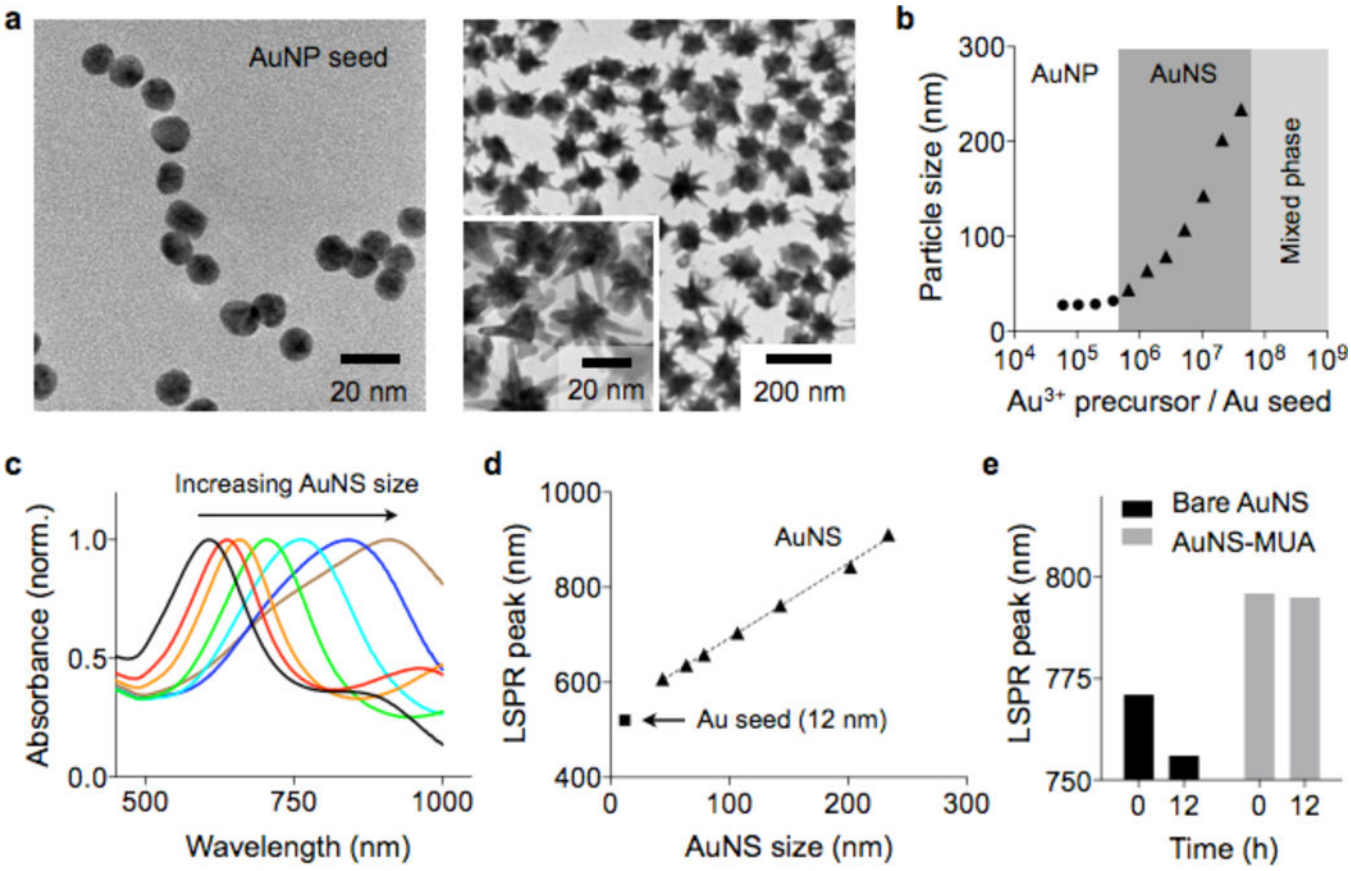

Figure 1.

Synthesis and characterization of AuNS. (a) Transmission electron microscopy (TEM) images of AuNP and AuNS. Spherical particles (diameter 13 nm, left) were used as a seed to grow AuNS (right). (b) The size of AuNS was controlled by changing the ratio between AuNP seed and Au^{3+} precursor concentrations. (c, d) Absorbance spectra of AuNS. Increasing the particle size led to shifts of the LSPR peaks to longer wavelengths. (e) Bare AuNS showed a drift in LSPR peak over time. Passivating the AuNS with a thiol ligand (11-mercaptoundecanoic acid/MUA) stabilized the LSPR spectra.

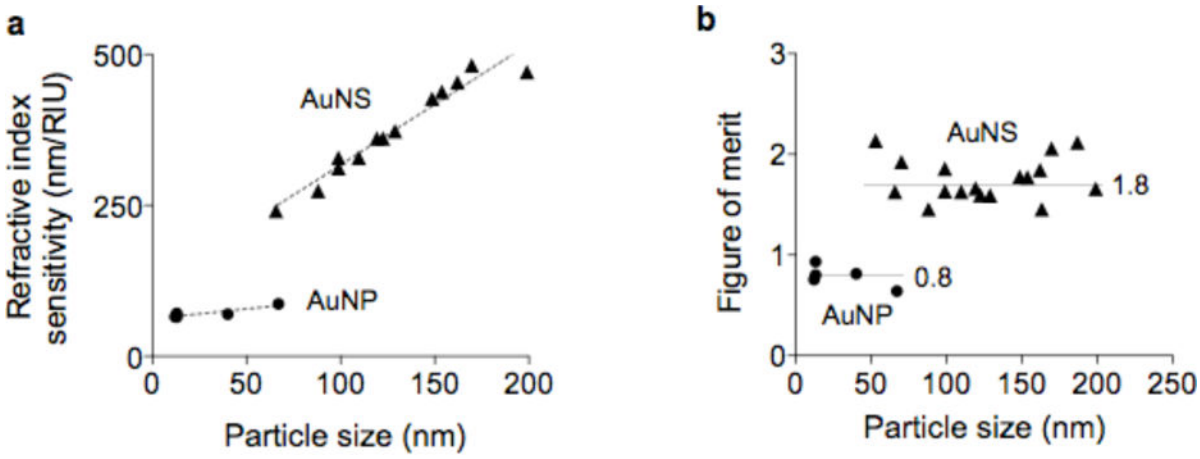

Figure 2.

Detection sensitivities of AuNP and AuNS. (a) The refractive index sensitivity (RIS) of AuNS and AuNP of different sizes was measured. The RIS linearly increased with the overall size of the particles. (b) The figure of merit (FOM) was obtained by dividing the RIS with the corresponding full width at half maximum of the LSPR peak. AuNS assumed higher FOM than AuNP. For a given particle type (i.e., AuNS or AuNP), the FOM values were found similar, independent of the particle size ($P = 0.87$, AuNS; $P = 0.18$, AuNP).

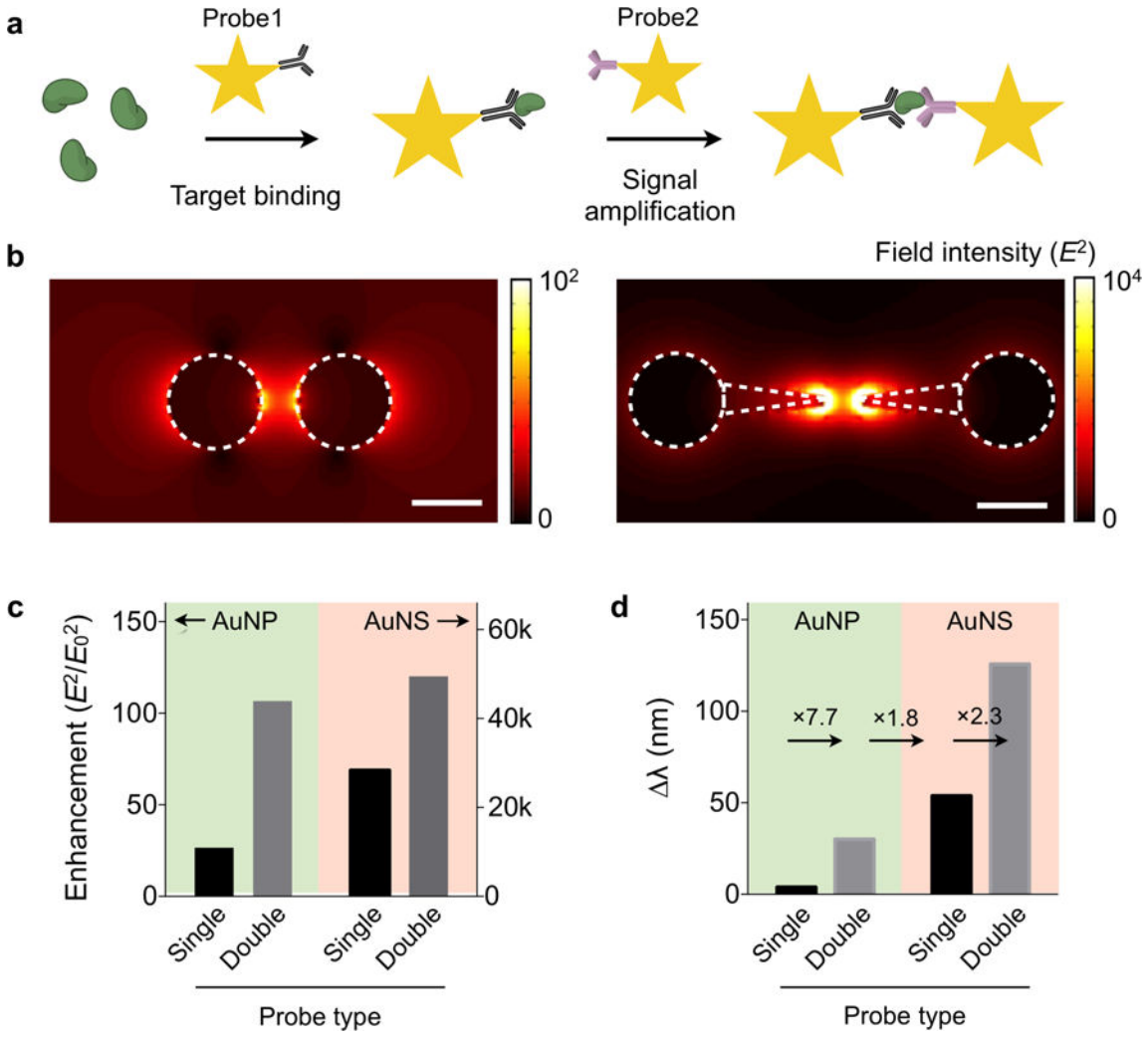

Figure 3.

Electromagnetic simulation of the clustering assay. (a) Schematic of the AuNS clustering assay. The target molecule bridges the metal tips of AuNS probes to concentrate electrical fields. (b) Simulated electric field (E) distribution surrounding a particle pair. The field magnitude is 460 times higher in the AuNS dimer (right) than in the AuNP dimer (left). Scale bar, 50 nm. (c) The field intensity (E^2) relative to that of the incident light (E_0^2) was compared for different assay configurations. The clustering assay amplifies the signal from the single-probe assay. (d) The spectral shift (Δλ) for each assay type was calculated from the E-field data. The overall sensitivity improved by >32 fold with the AuNS-clustering assay.

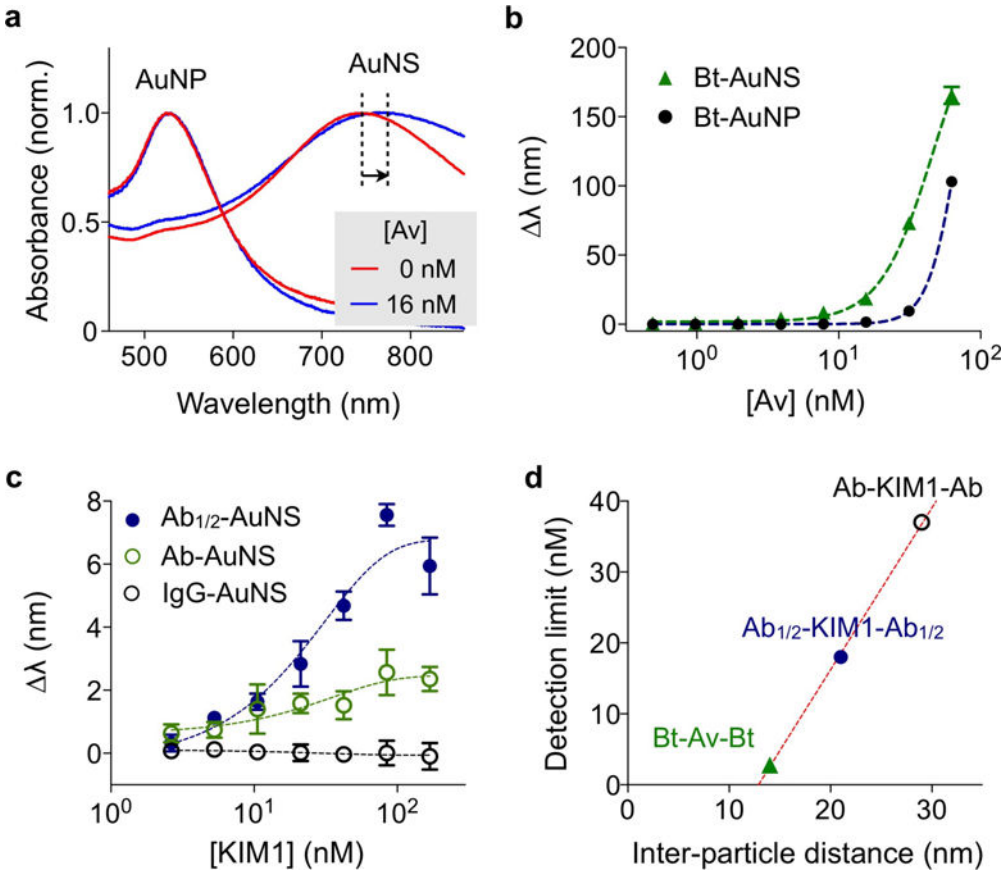

Figure 4.

Protein detection with AuNS. (a) Biotinylated AuNP (Bt-AuNP) and AuNS (Bt-AuNS) with similar particle volumes were incubated with avidin, and the corresponding spectral changes were monitored. With the addition of 16 nM of avidin, Bt-AuNS displayed more pronounced spectral shifts ($\Delta\lambda$ = 19 nm) than Bt-AuNP ($\Delta\lambda$ = 1.5 nm) (b) Avidin-titration experiments confirmed the superior sensitivity of the AuNS system. The limit of detection (LOD) of Bt-AuNS was 7 times lower than that of Bt-AuNP. (c) The effect of the inter-particle distance on the assay sensitivity was studied. Kidney injury molecule-1 (KIM1) was used as the detection target. To change the inter-particle distance, AuNS was conjugated with either full antibody against KIM1 (Ab-AuNS) or half-antibody fragments ($Ab_{1/2}$-AuNS). The shorter probe ($Ab_{1/2}$-AuNS) produced larger LSPR spectral shifts in KIM1 titration measurements. AuNS conjugated with isotype-matched goat IgG was used as control. (d) The detection limits of the three systems in (b) and (c) were compared. The detection sensitivity was found to be inversely proportional to the inter-particle distance.